PERFORMANCE OF A SUSTAINABLE ASPHALT MIX INCORPORATING HIGH RAP CONTENT AND NOVEL BIO-DERIVED BINDER

Journal:	*Road Materials and Pavement Design*
Manuscript ID	RMPD-19-02-24.R1
Manuscript Type:	Original Scientific Paper
Keywords:	RAP, Bio-Additives, Sustainable Pavements, Rejuvenation

PERFORMANCE OF A SUSTAINABLE ASPHALT MIX INCORPORATING HIGH RAP CONTENT AND NOVEL BIO-DERIVED BINDER

Nicholas D. Manke[a]*, R. Christopher Williams[b], Zahra Sotoodeh-Nia[c], Eric W. Cochran[d], Laurent Porot[e], Emmanuel Chailleux[f], Simon Pouget[g], Francois Olard[h], Ana Jimenez Del Barco Carrion[i], Jean-Pascal Planche[j], Davide Lopresti[k]

[a] *Doctoral Candidate, Iowa State University*
Department of Civil, Construction, and Environmental Engineering
174 Town Engineering, Ames, Iowa, 50011
nmanke@iastate.edu
[b] *Professor (Ph.D.), Iowa State University*
Department of Civil, Construction, and Environmental Engineering
486 Town Engineering, Ames, Iowa, 50011
rwilliam@iastate.edu
[c] *Doctoral Candidate, Iowa State University*
Department of Civil, Construction, and Environmental Engineering
427 Town Engineering, Ames, Iowa, 50011
znia@iastate.edu
[d] *Professor (Ph.D.), Iowa State University*
Department of Chemical, and Biological Engineering
3133 Sweeney, Ames, Iowa, 50011
ecochran@iastate.edu
[e] *Senior Staff Scientist, Kraton Corporation, Arizona Chemical*
Laurent.Porot@kraton.com
[f] *Senior Researcher (Ph.D.), IFSTTAR*
Department of Materials and Structures
emmanuel.chailleux@ifsttar.fr
[g] *Researcher (Ph.D.), EIFFAGE Infrastructures*
69964 Corbas Cedex, France
Simon.POUGET@eiffage.com
[h] *Director of Research & Innovation (Ph.D., HDR), EIFFAGE Infrastructures*
69964 Corbas Cedex, France
Francois.OLARD@eiffage.com
[i] *Research Fellow, University of Nottingham*
Department of Civil Engineering, Nottingham Transportation Engineering Centre
Room C20, Pavement Research Building, University Park, Nottingham, NG7 2RD
Ana.Jimenezdelbarcocarrion@nottingham.ac.uk
[j] *Senior VP Asphalt and Petroleum Technologies (Ph.D.), Western Research Institute*
3474 North 3rd Street, Laramie, Wyoming, 82072
jplanche@uwyo.edu
[k] *Principal Research fellow, University of Nottingham*
Nottingham Transportation Engineering Centre
Room C11, Pavement Research Building, University Park, Nottingham, NG7 2RD
Davide.Lopresti@nottingham.ac.uk

Word Count: 9652

KEYWORDS:

RAP, Rejuvenator, Bio-Binder, Sustainable Pavements

ABSTRACT

The recent drive to find ways to increase sustainability and decrease costs in asphalt paving has led researchers to find innovative ways to incorporate more recycled materials and bio-derived binders into mixes with varying success. A new novel bio-derived binder made from refined pine chemistry stabilized with a polymer can increase the sustainability of asphalt mixes while maintaining pavement performance. Laboratory performance testing was conducted on asphalt mixes containing 50% Reclaimed Asphalt Pavement (RAP) by mix weight and the novel bio-derived binder. Results show that the bio-derived binder outperforms the conventional 50/70 pen grade binder mixes with respect to resistance to thermal cracking and adequately passes all requirements for pavements with 20-year design loadings of less than 30 million ESALs. This research shows that asphalt mixes containing 50% RAP and a bio-derived binder can be designed to pass performance criteria at low, intermediate, and high temperatures without the need of neat bitumen.

I. INTRODUCTION

The current conditions of infrastructure around the world coupled with limited government funding and rising material and labor costs have increased the drive for finding ways to effectively cut paving costs by incorporating more recycled materials. Depleting sources of quality virgin aggregates and high and fluctuant crude oil prices lead to ever-increasing material costs in paving that can best be offset by partial or total replacement of conventional virgin materials in asphalt mixes. Additionally, maximizing the use of recycled materials is critical in terms of environmental cost savings related to aggregate quarrying. Reclaimed asphalt pavement (RAP), here being synonymous with RA in EU standards, has been used in asphalt mixes for decades and started becoming popular in the 1970s. Today, RAP is the most recycled material in the U.S. at over 80 million tons being re-used annually in paving, fill, and base material (FHWA, 2011; NCAT, 1991). Likewise, in Europe, more than 40 million tons of RAP is re-used each year (EAPA, 2016). However, RAP as a material is largely underutilized throughout the world by limiting specifications, lacking guidance, and hesitation to put laboratory findings into practice.

Much of the hesitation to allow high RAP contents in asphalt mixes is attributed to the stiffness of the aged binder introduced into the mix. Highly aged binders lose much of their flexibility and ability to dissipate stresses through viscoelastic relaxation making them susceptible to brittle failures such as fatigue cracking and low temperature thermal cracking. The increased stiffness does; however, have the positive influence of increasing the mix's resistance to high temperature shearing deformations like rutting and shoving. A critical balance must be made to increase or restore the ability to relax stress of the asphalt mix incorporating a high RAP content while retaining sufficient stiffness to resist rutting. Such a balance can be achieved through the use of RAP rejuvenation or utilizing a specifically designed binder as was done in this research.

Partial binder replacement by bio-derived materials has been a recent focus of numerous research studies to further increase the sustainability of asphalt pavements and lower paving costs. This research goes a step further by using an asphalt mix incorporating 100% conventional virgin binder replacement by reclaimed binder and a novel sustainable binder derived from refined pine chemistry stabilized with polymers. In addition to the use of no virgin crude oil-derived binder, the mix tested in this research incorporates 50% RAP by mix weight.

This research, as part of the BioRePavation project, is intended to show that in a post-fossil fuel scenario where crude oil is unavailable, economically unfeasible, or its extraction deemed unsustainable, bio-asphalt mixes manufactured with bio-derived binder and high RAP content can be successfully developed. The larger BioRePavation project is a multi-faceted study involving multiple universities and researchers to increase the sustainability of flexible pavements. This study provides evidence that even with no addition of neat bituminous binder, bio-asphalt mixes under investigation pass all applicable specifications for pavements designed with 20-year design loads of 10 to 30 million ESALs.

II. BACKGROUND

The push for greater degrees of sustainability in asphalt paving have been focused largely on two major categories of research: rejuvenation of recycled materials to successfully incorporate higher percentages of RAP in mixes, and partial crude oil-derived binder replacement by sustainably-produced binders from waste and/or recycled materials. There has been much research and implementation of the prior category, whereas the latter category has been less thoroughly explored. The novel sustainable binder presented in this research presents; however, the possibility for a complete conventional binder replacement along with incorporation of high RAP contents.

Recycled asphalt pavement (RAP) contains aged binder which has undergone chemical changes resulting in altered physical responses to loading. Oxidation, moderate polycondensation, and volatilization of asphalt fractions increases the ratio of larger, or associating, asphaltene molecules to smaller lubricating maltene molecules like saturates, aromatics, and resins (Hesham, 2015). The result of such changes is a much stiffer material with substantially reduced flexibility and elastic responses to stresses. The primary function of a rejuvenator is to rebalance the strong intermolecular associations of the large, often polycondensed, asphaltene molecular binder fraction (Haghshenas et al., 2016). Common rejuvenator types include paraffinic oils, aromatic extracts, naphthenic oils, tall oils, and bio-rejuvenators refined from natural resources such as rapeseed, linseed, and pine oils. Research has shown that properly designed rejuvenation can result in adequate HMA mix designs incorporating up to 100% RAP by aggregate weight (Zaumanis et al., 2014). Additionally, rejuvenators have been shown to increase pavement life by up to nine years in mixes containing RAP (Hesham, 2015). Rejuvenation; however, has a key uncertainty pertaining to mix completion of the virgin binder with the aged RAP binder and rejuvenator (Zaumanis et al., 2014). Incomplete blending known as “black rock” can lead to moisture damage, rutting, and premature cracking. Additionally, many agencies currently do not include rejuvenators in specifications or are hesitant to allow them due to the wariness that they may increase rutting and moisture damage potential (Haghshenas et al., 2016; Kowalski et al., 2017).

The rejuvenating effect and linear viscoelastic properties of bio-binders manufactured from pine resin and by-products of the paper industry in asphalt mixes with 50% RAP and bio-binders as the only virgin binder has also been investigated (Jiménez del Barco et al., 2017; Jiménez del Barco et al., 2017). The bio-binders showed great potential to rejuvenate RAP and the bio-recycled asphalt mixes had acceptable viscoelastic properties compared to conventional mixes while being composed only of RAP and non-petroleum-based binders.

These studies and more show that industrial and consumer waste products can be valuable resources in flexible pavement materials. Not only can the developed materials increase the sustainability of pavements by increasing the allowable quantity of recycled materials, but they can also allow for the partial or total replacement of crude oil-derived binders. The usage of otherwise waste materials not only offers promise of substantial material savings, but also

the real possibility of offering economic incentives to the industries producing the waste materials.

III. MATERIALS

Binders, aggregates, and RAP materials were provided by EIFFAGE, a paving contractor based in France, for this research. Binders used included a virgin 50/70 pen grade (PG 64-22) conventional binder as well as a novel bio-binder referred to as Biophalt® (BF). BF is derived from polymer-modified refined pine sap and does not contain any source of petroleum products other than the polymer (Biophalt Patent; Pouget and Loup, 2013). The RAP was delivered fractionated in coarse (8/12 mm) and fine (0/8 mm) fractions. Both the RAP and virgin aggregates were oven-dried and split to ensure uniformity of the materials in each mixed batch for preparing test specimens. RAP binder content was determined according to ASTM D 2172 (2007) and ASTM D 7906 (2007) standards. Each RAP fraction's binder content was determined individually by using toluene to dissolve the aged binder off of the aggregates and then using a series of centrifuges to separate the toluene-binder solution from the aggregates. A rotary evaporator was then used to distill the binder from the toluene. Because this paper focuses on mix performance comparisons, only a brief summary of material properties is included for reference.

Table 1 provides a summary of binder grades as determined using all applicable ASTM and AASHTO testing standards and following the Superpave methodology of binder grading using the performance grading (PG) system.

Table 1: Binder PG Grade Summary

Binder	PG Grade	Penetration (x0.1mm)	Softening point (°C)	Fraass breaking point (°C)
Control	PG 64-22	55.0	49.0	-7
BF	N/A*	146.5	73.5	-15
RAP	PG 94-4	6.5	81.0	+14
Control + RAP	PG 76-16	25.0	61.8	+1
BF + RAP	PG 58-22	80.0	68.8	-7

The BF binder was unable to be tested using the DSR due to the sticky nature of the virgin binder. However, the conventional characterization shows that it is a soft binder and the blended grade with RAP is significantly lower than the control, so it is reasonable to assume that the virgin BF binder has a high temperature grade softer than PG 58. By comparing the unblended and blender binder grades and conventional properties shown in Table 1, one can conclude that the BF binder lends itself well to use in mix designs containing high RAP contents.

IV. MIX DESIGN

To directly compare the effectiveness of the novel bio-binder, BF, with the control binder, mix designs for all performance testing were controlled to consist of the same binder contents and aggregates. Mixes for both binders contained 50% RAP by aggregate weight, 2.7% virgin binder by mix weight, and 1.7% recycled binder by mix weight.

Table 2 summarizes the aggregate gradations for virgin aggregate, blended RAP fractionations, and the final design aggregate blend used in all performance test mixes. The blend gradation is designed based on aggregate packing volumetric concepts to optimize interlock and densities. Minimum and maximum requirements are as suggested by the Superpave mix design methodology. It should be noted that these gradations were used for laboratory-prepared mixes and a slightly different gradation curve was used for large-scale field testing. However, the focus of this study is on the comparison of the binders, so only the consistency of the gradations among mix sub-groupings is of importance for validation of subsequent comparative results.

Table 2: Aggregate Gradations

Sieve Size		Percent Passing			Requirements	
U.S. Customary	mm	Virgin	RAP	Blend	Min	Max
1”	25	100	100	100.0	100	
3/4”	19	98.9	99.9	99.4	90	100
1/2”	12.5	66.9	92.4	80.0		90
3/8”	9.5	29.6	60.6	45.5		
#4	4.75	23.5	29.9	26.8		
#8	2.36	22.6	24.7	23.7	23	49
#16	1.18	17.1	7.6	12.2		
#30	0.60	12.9	3.6	8.1		
#50	0.30	10.0	1.3	5.5		
#100	0.15	8.1	0.4	4.1		
#200	0.075	6.6	0.1	3.2	2	8

The nominal maximum aggregate size (NMAS) of the design blend is 19.0 mm which increases surface friction and mandates a minimum pavement lift thickness of 76 mm (3 inches) (Asphalt Institute, 2014).

All specimens prepared for performance testing were mixed in small batches in the laboratory, short-term oven aged, and subsequently compacted using a gyratory compactor. The volumetric properties of mixes using each binder were tested against Superpave requirements for 20-year design ESAL ratings in excess of 10 million but less than 30 million (Asphalt Institute, 2014). Table 3 provides a summary of all tested and calculated volumetric properties of primary importance for each mix. AASHTO T 331 (2015) testing standards

using the CoreLok method were used to determine mix bulk specific gravities (G_{mb}), while maximum theoretical specific gravities (G_{mm}) of mixes were determined according to the AASHTO T 209 (2015) specification.

Table 3: Mixture Volumetrics

Property	Control	BF	Requirement
P_b	4.49	4.49	-
P_b (virgin)	2.8	2.8	-
P_b (RAP)	1.69	1.69	-
VMA	13.2	14.2	>13.0
VFA	69.5	71.6	65-78
DP	0.7	0.6	0.6-1.2
P_{ba}	0.8	0.4	-
P_{be}	3.7	4.1	-
G_{mm}	2.63	2.60	-
G_{mb}	2.52	2.50	-
$\%V_a$	4.0	4.0	4.0
G_b	1.047	1.035	-
G_{se}	2.831	2.799	-
G_{sb}	2.778	2.778	-

As is shown in Table 3, both mix designs meet all applicable Superpave mixture volumetric requirements for pavements with 20-year design loads in excess of 10 million but less than 30 million ESALs. Slight variations in mix volumetrics consisting of the same relative gradations and binder contents is most likely attributable to the variation of the binder absorption into aggregate surface voids and binder specific gravity. Using the standard ESAL equations and associated factors attributable to an urban arterial or highway, a 20-year design load of 30 million ESALs equates to approximately 27,500 to 32,500 vehicles/day whereas a 10 million ESAL design load equates to approximately 7,500 to 12,500 vehicles/day as an idea for associative traffic levels being discussed. These estimates are based on back-calculations from Equation 1 (Huang, 2004).

$$ESAL=(ADT)_0(T)(T_f)(G)(D)(L)(365)(Y) \quad [Eq.1]$$

where:

$(ADT)_0$ = average daily traffic at the start of design period (veh/day)
T = percentage of trucks as a decimal (varied)
T_f = truck factor (varied)
G = traffic growth factor (varied from 2% to 5% growth rate)
D = directional distribution factor (assumed to be 0.5)
L = lane distribution factor (assumed to be 1; two-lane highway)
Y = design period in years (assumed to be 20)

V. PERFORMANCE TESTING

Several types of testing were carried out on laboratory-mixed and compacted specimens to assess the performance of the novel bio-binder in comparison to a standard crude oil-derived binder. Because asphalt mixes contain viscoelastic materials, it is important to test mixture performance at a variety of temperatures and loading conditions to ensure the pavement can withstand a wide variation of environmental and traffic loading conditions in the field. Disc-shaped compact tension (DCT) testing was chosen to assess the asphalt mixes' resistance to low temperature thermal cracking while beam fatigue testing was selected to assess their resistance to intermediate temperature fatigue cracking. To predict high temperature rutting resistance, flow number testing was used. Additionally, dynamic modulus testing was used to construct master curves and indirect tension testing was used to assess moisture susceptibility.

A. TESTING PROCEDURES

A.1. Disc-Shaped Compact Tension (DCT)

Low-temperature thermal cracking is a distress initiated by environmental loading effects. In geographic areas where daily and annual thermal fluctuations can be extreme, thermal cracking in pavements can significantly increase the required maintenance of the pavement and/or shorten the lifespan of the pavement. As temperatures decrease, pavements shrink dimensionally generating significant tensile stresses within the system. At very low temperatures, tensile stresses can exceed the tensile strength of the pavement resulting in cracking (Huang, 2004). Thermal cracking is typically transverse to travel direction and is top-down in nature due to the more rapid surface cooling, geothermal heating and thus thermal gradation that exists within a pavement cross-section in cold weather (NCAT 1991). Cyclic thermal fluctuations exacerbate micro-fractures and cold weather loading further deteriorate the distress due to the brittleness of binders at low temperatures. While thermal cracking is typically not associated with traffic loading, the presence of transverse thermal cracks in short intervals allows for moisture penetration into the subgrade and general discontinuity of the pavement system to effectively distribute loading.

Disc-shaped compact tension (DCT) testing was performed in accordance with ASTM D 7313 (2007) procedural standards to assess the low temperature tensile strength of the mixes. Three specimens were prepared for each test subset as outlined in Table 4.

Table 4: DCT Testing Subset Parameters

Binder	% Air Voids	Test Temperature (°C)
Control	4	-6
	7	-6
	7	-12
BF	4	-12
	7	-12

Specimens were tested at four percent air voids to assess the resistance to thermal cracking after considerable traffic loading and at seven percent air voids to assess performance at construction. Control mixes were tested at both -6 and -12°C because the binder low performance grade of the control mix (-16°C) varied from that of the BF mix (-22°C). ASTM standards suggest DCT testing to be performed at 10°C greater than the low grade of the binder; however, the control mix was also tested at -12°C as a direct comparison to the BF mix under the same environmental conditions.

Each specimen was laboratory-mixed and compacted using a Superpave gyratory compactor. Compacted specimens were then cored using a water-cooled drill press and cut using water-cooled saws. Prepared specimens were of the dimensions and configuration shown in Figure 1 as provided in ASTM D 7313 (2007).

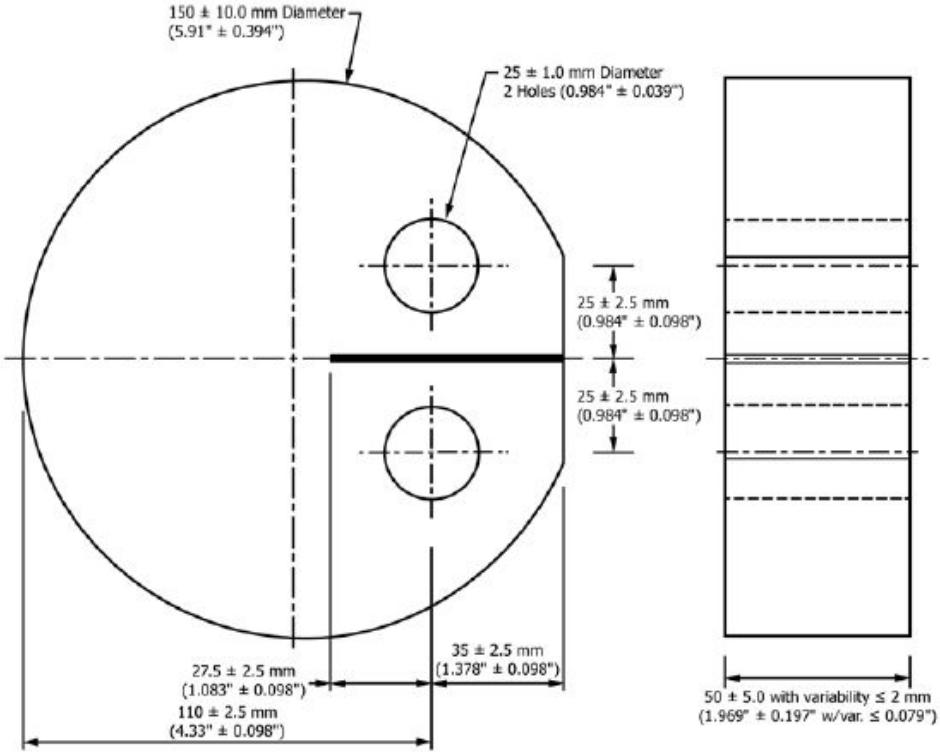

Figure 1: ASTM Standard DCT Specimen Dimensions (ASTM D 7313)

Prepared specimens were allowed to dry at room temperature for a minimum of 24 hours and fitted with metal gauge points. Air-dried specimens were then conditioned at the test temperature in an environmentally-controlled unit for 8 to 16 hours prior to testing in an environmentally-controlled testing apparatus. A crack mouth opening displacement (CMOD) gauge was clipped into the metal gauge points and the specimen was loaded to failure at a controlled CMOD rate of 0.0017 mm/sec. The failure criteria was the point at which tensile load resistance was reduced to less than 0.1 kN.

Data collected included CMOD versus loading. The data plotted to specimen failure was then used to calculate the fracture energy (G_f) of each specimen using Equation 2 and normalized to individual specimen dimensions.

$$G_f = A_f/(l*t) \quad \text{[Eq.2]}$$

where:

A_f = Area under the load vs. CMOD plot (J),
l = Length of the fractured face (m), and
t = Specimen thickness (m).

A.2. Beam Fatigue

Beam fatigue results are useful in predicting the fatigue behavior of HMA mixes. Fatigue cracking is attributed to high loading repetitions at temperatures intermediate relative to the environment the pavements are placed and is thus linked to the effective binder grade of the mix. Effective binder grade in this instance refers to the blended binder grades of both virgin binder and RAP binder in the respective mixes. The significance of predicting fatigue behavior at intermediate temperatures is that these conditions dictate the working conditions the pavement will be subjected to through much of its life. Fatigue cracking begins as top-down or bottom-up micro fractures that develop through repeated strain cycling as flexible pavements deflect and recover through loading-unloading cycles. As cracking evolves, it isolates sections of the pavement from the system which accelerates pavement deterioration and results in the familiar alligator skin-like pattern of interconnected fractures.

Beam fatigue testing was completed in accordance with AASHTO T 321 (2017) procedural standards. For each binder, six beams were made with the following nominal dimensions: 380 mm in length x 63 mm in width x 50 mm in thickness. Sets of six beams were cut from two slabs (three beams per slab) made at seven percent air voids and compacted using a linear kneading slab compactor. Slabs were oversized in width to ensure each beam consisted of two saw-cut edges. Prepared beams were then normalized in an environmentally-controlled chamber with the testing device at a temperature of 20°C. Specimens were then loaded individually into a four-point flexural bending apparatus and axially haversine loaded at a frequency of 10 Hz. Figure 2 shows a sample beam in the testing device used as a reference.

Figure 2: Beam Fatigue Testing Apparatus

Tests were run in strain control mode on each individual beam, with the group of six beams for each binder/mix combination generating one data set for analysis covering varying strain amplitude levels. Strain control mode loading is more relevant to performance of thin pavement layers less than 130 mm (5-inches) in thickness since the mechanical response is driven by the soil stiffness in this case (NCAT, 1991). The six strain amplitude levels chosen ranged from 1200 to 300 micro-strain. Data collected for analysis were the strain level and cycles to failure which is described by AASHTO T 321 (2017) as the maximum value of the product of measured flexural stiffness and number of load cycles during testing. The failure criteria was 50% of the initial flexural stiffness determined at the 50th load cycle. Fifty load cycles ensured the beams were appropriately seated and thus the initial flexural stiffness is representative. Strain and load cycles to failure can be plotted on a log-log plot to determine best-fit flexural coefficients K1 and K2 described using the following power law relationship.

$$N_f = K1\left(1/\epsilon_0\right)^{K2} \quad \text{[Eq. 3]}$$

where:

N_f = number of load cycles to failure,

ε_0 = flexural strain amplitude in micro-strain, and

K1, K2 = regression constants.

A.3. Flow Number

The most common type of high temperature distress in flexible pavements is rutting. Rutting can occur as a result of a weak subgrade or shear deformation of the asphalt mix itself under loading. The latter mode is in part the focus of this research. Although the incorporation of RAP with its stiff, aged binder typically increases a pavement's resistance to rutting, the influence of a non-conventional binder on rutting resistance is of interest. A mix's susceptibility to rutting is dependent on both aggregate characteristics (i.e. angularity, gradation, etc.) and the binder's properties including shear modulus. Because the same aggregate sources were used for both mixes in this study, any variation in rutting resistance can be attributed to binder effects.

Flow number testing was performed on four specimens per mix in accordance with AASHTO T 378 (2017). Test specimens were previously used to conduct non-destructive dynamic modulus testing. Testing was completed using a UTM 25 asphalt mixture performance tester (AMPT) at a controlled temperature of 54°C under unconfined conditions. Each specimen was compacted to 7% air voids using a Superpave Gyratory Compactor to the specified nominal dimensions of 100-mm in diameter by 150-mm in height. An air void content of 7% is representative of the upper threshold of many conventional mixes post-construction. Samples were subjected to a 600 kN haversine axial compression load at a frequency of 1 Hz. Each load cycle consisted of a 0.1 s load pulse followed by a 0.9 s rest period. Tests were ended once the specimen reached 5% permanent axial strain or 10,000 load cycles, whichever occurred first. Reported results included the flow number of each specimen which is defined as the load cycle corresponding to the minimum permanent strain rate per cycle. The flow number (FN) is usually considered to be the onset of tertiary flow, or creep within the specimen and is a measurement of matrix shearing under repetitive loading cycles.

During flow number testing, an asphalt specimen can undergo three phases of deformation: primary, secondary, and tertiary. Primary deformation is the initial consolidation of voids and other preliminary densification phenomena. Secondary deformation is the viscoelastic response consisting of deformation-relaxation cycles. Tertiary deformation is a plastic, or creep response of the specimen indicating shear failure. Figure 3 shows a plot of accumulated permanent strain and strain rate per cycle vs. load cycles and the three phases of deformation. The results shown in Figure 3 are an illustrative example.

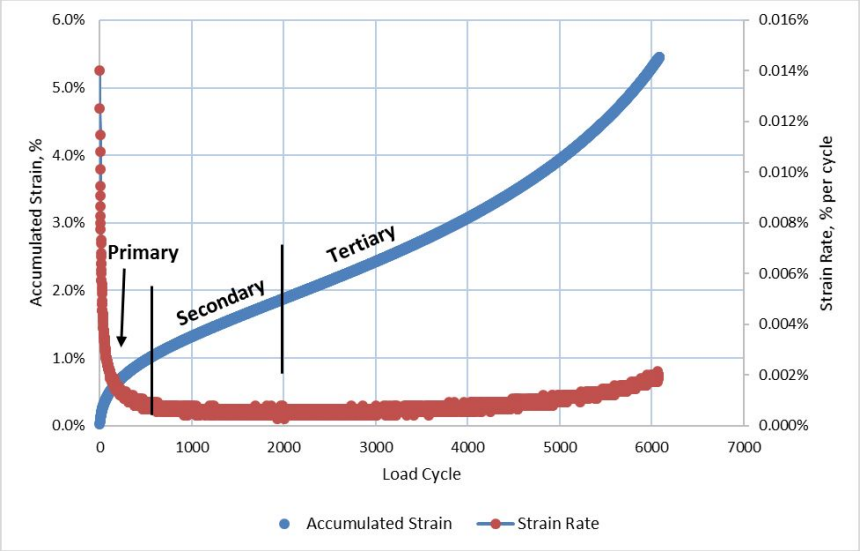

Figure 3: Example of Deformation Under Loading

A.4. Dynamic Modulus

Dynamic modulus testing was used in accordance with AASHTO TP 79 (2013) specifications to determine the stress-strain behavior of the mixes over a wide range of temperatures and frequencies in the linear viscoelastic domain. Recorded dynamic modulus values (E*) over the range of temperatures and frequencies were used to construct sigmoidal master curves. Master curves show how the mix's stiffness varies with loading rates. At low temperatures and high frequencies, pavements are more susceptible to brittle cracking failures. At high temperatures and low frequencies, pavements are more susceptible to viscous shear failures like rutting. At intermediate temperatures and frequencies, pavements are most susceptible to fatigue cracking where a moderate stiffness balancing deformation-resistance and elasticity to prevent brittle failure is desired. Master curves can therefore help predict pavement distressing problems over a wide range of scenarios.

Each test subset consisted of four specimens except for five control mix specimens tested at 7% air voids. There were four subsets: each mix compacted to 4% and 7% air voids. Each specimen was compacted to nominal dimensions of 100 mm in diameter and 150 mm in height using a Superpave gyratory compactor. Specimens were then subjected to sinusoidal axial loading to a reference stress using a universal testing machine (UTM) in a temperature-regulated chamber. Specimen axial strains were measured using linear variable differential transformers (LVDTs). Three temperatures (4, 21, and 37°C) and eight frequencies (25, 10, 5,

2, 1, 0.5, 0.2, and 0.1 Hz) were used to construct subsequent master curves for each data subset.

Master curves were plotted using frequencies shifted to an intermediate reference temperature of 21°C and plotted on a log-log scale to form sigmoidal curves. Curves were fitted using both the shifted data from the dynamic modulus testing as well as predicted curves for extrapolation of trends at frequencies beyond those tested. Predicted curves are best-fit sigmoidal functions that minimize standard error between actual and predicted stiffness values through the reduced frequency sections for which data is available. The sigmoidal function used can be seen in Equation 4.

$$Log|E^*| = a + \frac{b}{1+e^{\beta+\gamma(\log f_R)}} \quad \text{[Eq. 4]}$$

where:

f_R = reduced frequency at reference temperature in Hz,
a = minimum value of E* in MPa,
a + b = maximum value of E* in MPa, and
β, γ = fitting coefficients.

A.5. Moisture Susceptibility

Moisture damage is a common problem for pavements, especially those in areas where seasonal freeze-thaw cycles are prevalent. Due to aggregates' higher affinity for water than binder, water is able to diffuse through thin aggregate coatings and break the bonds between aggregates and binder. This type of damage is adhesive damage; however, cohesive damage is also possible as water molecules diffuse into the binder and soften it. Compounding moisture damage is the opening of surface shrinkage microcracks due to differential surface binder aging, pore pressures generated within air voids upon loading cycles, and hydrostatic pressures within saturated air voids from volumetric expansion as water freezes. While there is no consensus agreement among agencies and researchers about how RAP use in asphalt mixtures influences moisture resistance, some claim that high RAP contents generally improve a mix's moisture resistance (Haghshenas et al., 2016). Moisture resistance improvement is attributable to the pre-coating of hardened binder on aggregates that do not fully diffuse with the added virgin binder. A resulting thicker coating of binder of high viscosity should reduce the amount of adhesive (stripping) damage that occurs within the mix as moisture cannot diffuse across the thicker aggregate-binder interface (NCAT, 1991).

Moisture damage susceptibility of both mixes were assessed in accordance with AASHTO T 283 (2015) standards. This method subjects one set of specimens to a freeze-thaw cycle (wet) while one set remains unsaturated (dry). Specimens were lab-mixed and compacted to dimensions of 100 mm in diameter by 60 mm in height using a gyratory compactor. Each specimen was compacted around a target air void (AV) content of 7% to assess early-life moisture resistance. Once conditioned, specimens were loaded to failure in indirect tension at a displacement rate of 50 mm/min. Failure was deemed to be the point at which the specimen fractured, and load resistance fell below the recorded peak load. Peak loads were converted to peak strengths (kPa) by using specimen nominal dimensions. Using wet and dry peak

strengths of specimens of comparable air void contents, the tensile stress ratio (TSR) can be evaluated using Equation 5 and is an indicator of moisture damage susceptibility.

$$TSR = \frac{S_1}{S_2} \quad \text{[Eq. 5]}$$

where:

S_1 = peak strength of the wet conditioned specimen in kPa, and

S_2 = peak strength of the dry unconditioned specimen in kPa.

B. Testing Results

B.1. Disc-Shaped Compact Tension (DCT)

The DCT test results for each mixture parameters tested are summarized in Table 5.

Table 5: DCT Results Summary

Binder	Air Voids (%)	Test Temp. (°C)	Average G_f (J/m²)	CV, G_f (%)	Average Peak Load (kN)
Control	4	-6	624	22.7%	3.77
BF	4	-12	599	23.6%	3.55
Control	7	-6	717	8.2%	3.73
Control	7	-12	383	9.8%	3.25
BF	7	-12	581	18.0%	4.11

Table 5 shows the variation in average fracture energies, peak loads, and fracture energy coefficient of variation (CV). The CV is a statistical measure of data point dispersion where lower CVs indicate less scatter. To put the fracture energies presented in Table 2 into context, a comprehensive study has shown that G_f values greater than 400 J/m² indicate low potential of widespread thermal cracking within pavements (Buttlar et al., 2010). Only the control mix tested at -12°C and 7% air voids resulted in an average fracture energy below the 400 J/m² value. Peak load values are presented but not statistically compared due to the large standard deviations observed and relative closeness of values among mixes. Statistical comparisons among the mean fracture energies between mixes at comparable conditions are summarized in Table 6.

Table 6: Statistical Comparison Summary Between Mixes

Binder	Air Voids (%)	Test Temp. (°C)	Average G_f (J/m²)	P-value (ANOVA)	95% C.I. for $\mu_{Control}$-μ_{BF}
Control	4	-6	624	0.8349	(-295, 346)
BF	4	-12	599		
Control	7	-6	717	0.1192	(-55, 329)
BF	7	-12	581		
Control	7	-12	383	0.0365	(-376, -20)
BF	7	-12	581		

Table 6 shows comparative statistics among binder subsets' average fracture energies. One-way analysis of variance (ANOVA) p-values were calculated for differences among

compared means with lower values indicating higher probability of difference. The only statistically significant differences in means occurs at 7% air voids. The control mix tested at -6°C shows a somewhat significantly greater mean measured fracture energy than the BF mix tested at -12°C. When both mixes were tested at -12°C, the BF mix shows a strongly statistically significant difference between mean measured fracture energies, with the BF mix being the greater of the two. In addition to ANOVA p-values, 95% confidence intervals (C.I.) for mean differences are shown.

The second and third set of comparisons are important because it shows variation between binder performance when the mixes are tested at the same temperature and at temperatures 10°C greater than their respective low binder grade. When tested 10°C above their respective low binder grade, results show that the control mix will provide mean fracture energy values greater than those of the BF mix at roughly 88% confidence. When tested at the same temperature (-12°C), the BF mix will provide mean fracture energy values greater than those of the control mix at over 95% confidence.

In addition to comparisons between the mixes, comparisons were also analyzed within each mix. These investigations show mean fracture energy variations within mixes at varying air voids and test temperatures. Table 7 provides a summary of within mix statistical analyses.

Table 7: Statistical Comparison Summary Within Mixes

Binder	Air Voids (%)	Test Temp. (°C)	Average G_f (J/m^2)	P-value (ANOVA)	95% C.I.
Control	4	-6	624	0.3525	$\mu_{Cl4\%}-\mu_{Cl7\%}$ (-339, 153)
Control	7	-6	717		
Control	7	-6	717	0.0011	$\mu_{Cl-6}-\mu_{Cl-12}$ (223, 446)
Control	7	-12	383		
BF	4	-12	599	0.8676	$\mu_{BF4\%}-\mu_{BF7\%}$ (-263, 299)
BF	7	-12	581		

Table 7 shows that the only statistically significant difference in mean fracture energies within mixes occurs between the control mix when tested at -6°C and -12°C. However, by looking at the differences between mixes tested at 4% and 7% air voids, one can see that there is a greater likelihood of the control mix mean fracture energy decreasing as voids decrease during compaction through field loading. The BF mix; however, slightly increases in mean fracture energy with densification indicating sustenance of its resistance to thermal cracking throughout the pavement's life.

B.2. Beam Fatigue

A power law relationship was used to determine K1 and K2 values for each binder. Figure 4 shows the log-log plot used to determine the best-fit regression constants for each binder.

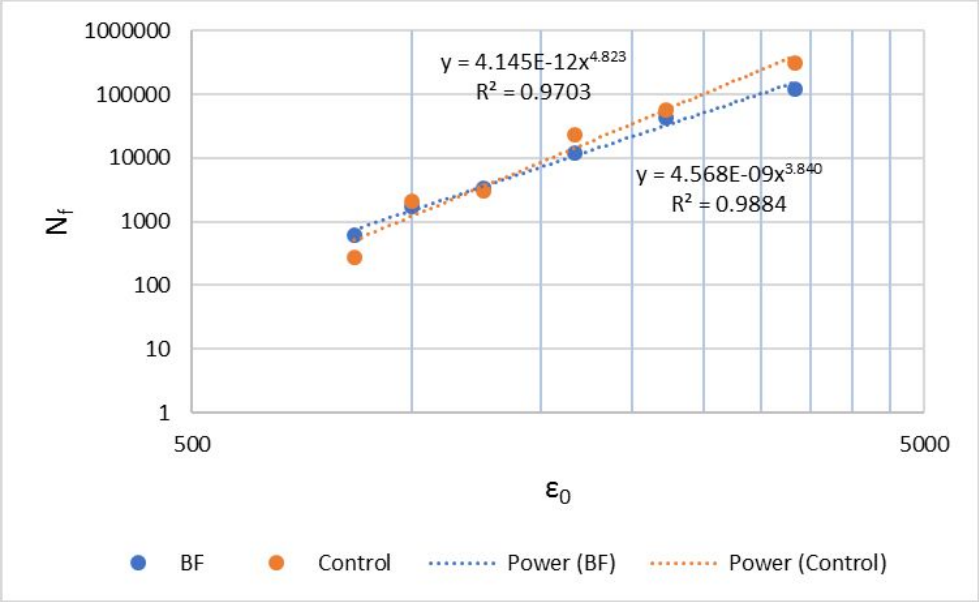

Figure 4. Fatigue Coefficient Determination

Results of Figure 4 are summarized in Table 8 for the important values under consideration.

Table 8. Fatigue Coefficients

Binder	K1	K2	R^2
Control	4.145E-12	4.823	0.9703
BF	4.568E-09	3.840	0.9884

As seen in Table 8, testing of both binders result in very small K1 values and high coefficient of determination values (R^2) close to unity signifying that the best-fit models account for 97.0% and 98.8% of the variance in predicted load cycles to failure for control and BF binders, respectively. The K2 fatigue exponent is indicative of damage rate accumulation within a beam specimen (Cascione et al., 2011). Due to the exponential nature, lower K2 values show a quicker rate of damage accumulation. Recommended values of K2 are based on laboratory prepared specimens and include 4.32 by the Transport and Road Research Laboratory to 4.76 by the Belgian Road Research Center (Huang, 2004). A K2 range of 3.5 to 4.5 was recommended to the Illinois Department of Transportation by Carpenter (Carpenter, 2006). It therefore stands that acceptable K2 values lie in a range of about 3.5 to 4.76 with more agencies recommending a K2 value of 4.0 or greater. Both binders tested provide reasonable K2 values ranging from 3.8 to 4.8 with the BF mix showing potential for a slightly faster rate of fatigue damage accumulation than the control.

Beam fatigue test results were also used to generate fatigue curves for the two binders considered. Figure 5 shows both curves on the same log-log plot for ease of comparison.

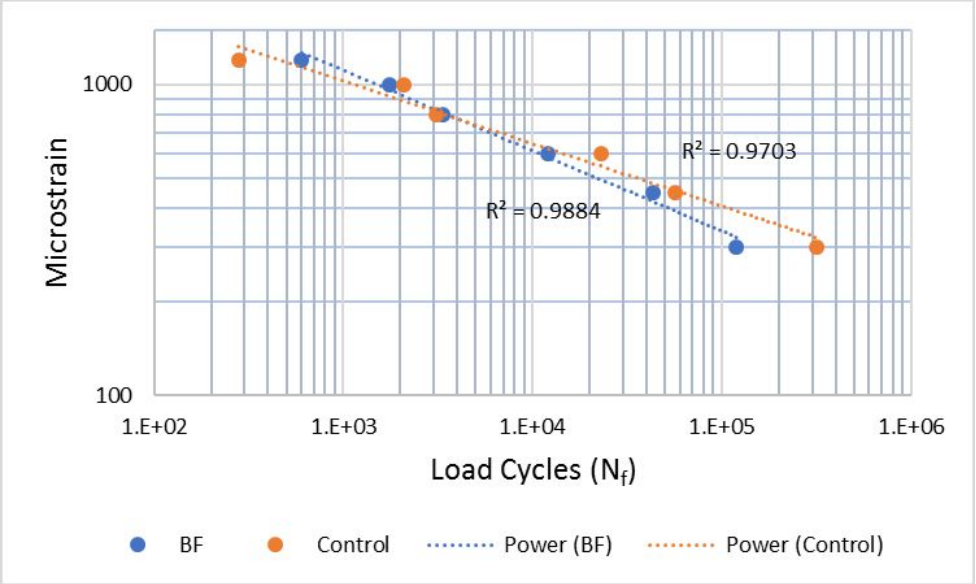

Figure 5. Fatigue Curves

Figure 5 shows that both binders have very similar fatigue curves with the BF mix having the slightly steeper slope due to the lower K2 value. The fatigue curve similarity indicates that both binders offer similar fatigue cracking resistance in the mixes tested. While each dataset of six beams was not repeated for statistical analysis in this study, the R^2 value of near unity for each dataset shows a desired log-log linearity and sufficient fatigue coefficient precision using a best-fit power trendline.

Figure 6 shows typical mix stiffness dissipation with progressive loading cycles at flexural strain amplitudes of 600 and 1000 micro-strain. These curves allow one to further assess the slightly lower K2 value determined for the BF mix and therefore more rapid rate of damage accumulation.

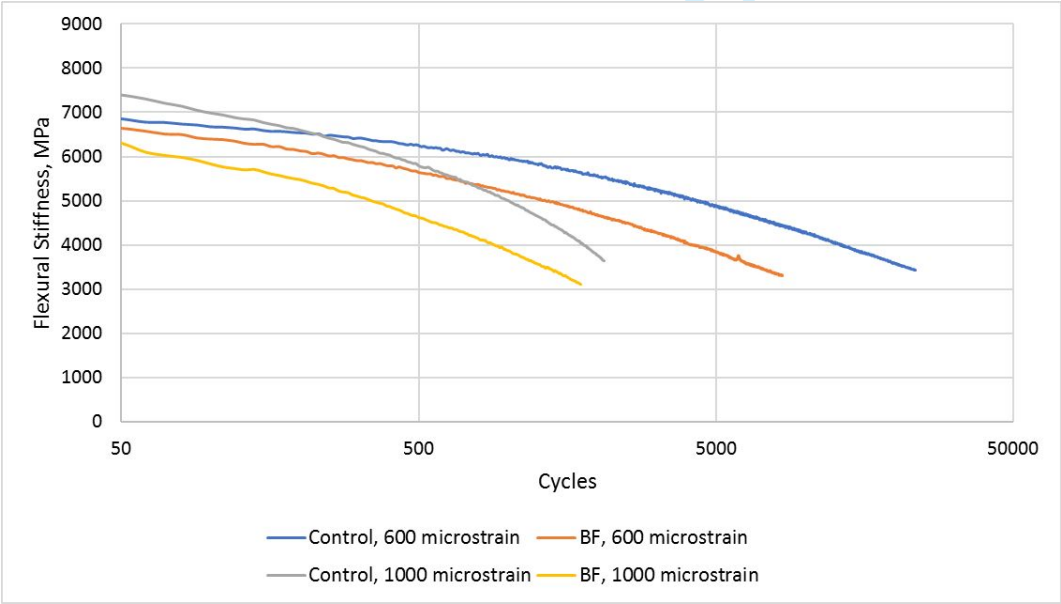

Figure 6: Flexural Stiffness Dissipation with Load Cycle Accumulation

Figure 6 clearly shows that the BF mix exhibits a more rapid rate of flexural stiffness dissipation with load cycles as compared to comparable control mixes. This observation is in agreement with the K2 evaluation predicting a more rapid rate of damage accumulation for the BF mixes. These phenomena are likely explained by the more viscous response under load at intermediate temperatures by the BF mix. More viscous behavior within a mix under repeated load cycles will generate internal heating that will further lower the flexural stiffness and account for a more rapid rate of damage accumulation and flexural stiffness dissipation.

B.3. Flow Number

Flow number test results and accompanying statistical summaries for each mix are provided in Table 9. In addition to the average FN for each mix, FN coefficient of variances (CV) are shown as a measure of data dispersion.

Table 9: Statistical Comparison Summary

Binder	Average FN	CV, FN (%)	P-value (ANOVA)	95% C.I. for $\mu_{Control}$-μ_{BF}
Control	863	6.2%	0.0050	(123, 447)
BF	578	20.9%		

As seen in Table 9, the control mix specimens had a greater average FN than the BF mix as well as a much lower CV meaning that control mix specimen measured FNs exhibited about one-third less data dispersion than the BF mix specimens. A one-way analysis of variance (ANOVA) was used to test the difference in mean FNs between the mixes. As shown, the comparison results in a p-value of 0.0050 indicating that the control mix mean FN is statistically significantly greater than that of the BF mix. A 95% confidence interval (C.I.) for the mean difference is shown to be between 123 and 447 load cycles.

The difference in mean flow numbers as well as the large variances observed for the BF mix specimens is most likely attributable to the difference in respective binder high temperature grades (see Table 1). A significantly softer BF binder + RAP binder at high temperatures relative to the control binder + RAP binder is expected to result in the observations found here. Additionally, the softness of the BF binder and the relatively high air void content of 7% may have also led to some additional lowering of the flow number. However, from a purely comparative standpoint of these two binders, the trends observed here are only meant to show that under the same conditions, the BF mix has slightly less resistance to rutting than the control mix as it pertains to flow number testing.

While the control mix had greater mean FN values, and subsequently greater resistance to rutting by shear deformation than the BF mix, it is important to analyze the mean FNs in terms of acceptable design ESALs each mix is suitable for. Table 10 shows recommended minimum FN values for varying degrees of design ESAL ratings (NCHRP, 2011). These recommendations are compared with 95% C.I.s for each mix's mean FN.

Table 10: NCHRP Recommended FN Values (NCHRP Report 673, Table 8-20)

ESALs (Millions)	Minimum FN	Control 95% C.I. μ_{FN}	BF 95% C.I. μ_{FN}
<3	-	(779, 948)	(386, 771)
3 to <10	53		
10 to <30	190		
≥30	740		

As seen in Table 10, the control mix provides acceptable rutting resistance based on flow number testing to qualify for design traffic loadings in excess of 30 million ESALs with 95% confidence based on these results. The BF mix is shown to qualify for design traffic loadings up to but not exceeding 30 million ESALs with 95% confidence based on these results.

B.4. Dynamic Modulus

Dynamic modulus (E*) values and subsequent sigmoidal master curves are compared both between and within mixes at 4% and 7% air voids. The dynamic modulus of a mix is the absolute value of the complex modulus and includes both the elastic stiffness and internal damping component generated by the viscoelastic binder (Huang, 2004). Master curves for both mixes compacted at 4% air voids shifted at a standard intermediate reference temperature of 21°C are shown in Figure 7 which reflects expected mix response after post-construction consolidation without considering binder aging effects. Also shown in Figure 7 are mix phase angles over the reduced frequencies tested. Phase angles are an indication of viscous or elastic behavioral response to loading with lower phase angles indicating more elastic (stress relaxation) responses and greater phase angles indicating more viscous (plastic deformation) behavior.

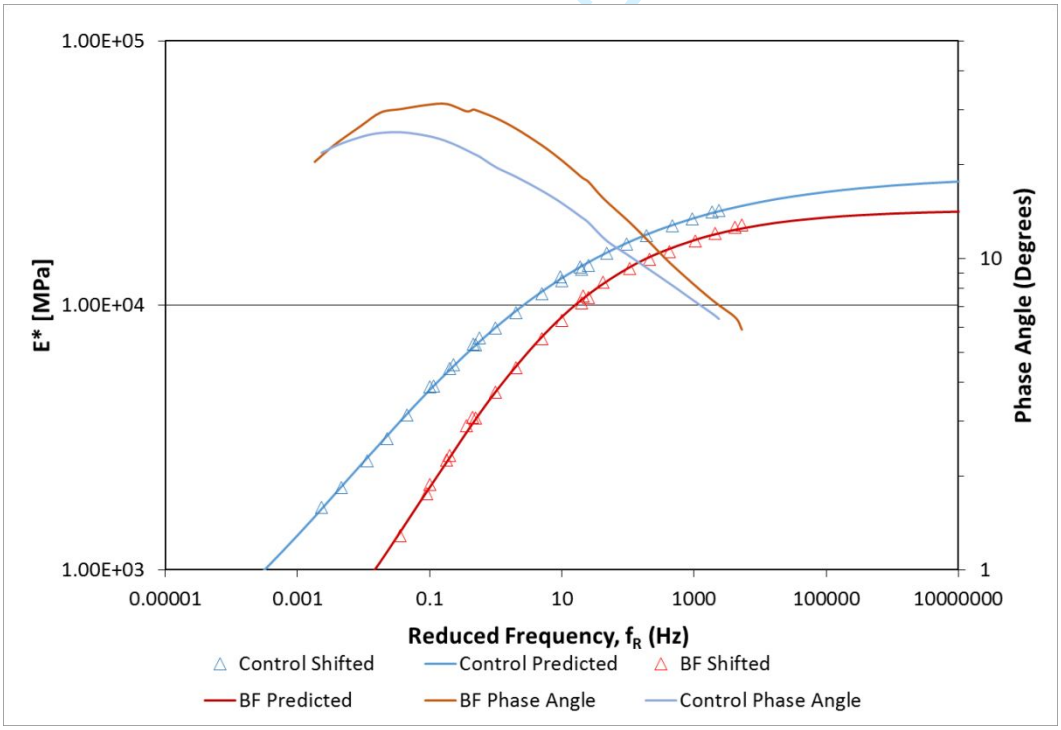

Figure 7: Mix Master Curves at 4% Air Voids

Figure 7 shows that the control mix displays greater stiffnesses than the BF mix over all frequencies at 4% air voids. The greater gap at low frequencies indicates that the control mix may provide greater rutting resistance at high temperatures where low loading frequencies are critical. The control mix's greater stiffness at high frequencies indicates that the control mix may be more prone to thermal cracking distress due to the more brittle behavior associated with high stiffnesses at low temperatures (NCAT, 1991). Select frequencies and temperatures were selected for statistical comparisons between the two mixes. Results are shown in Table 11.

Table 11: Summary Statistics Between Binders at 4% Air Voids

Binder	Temp. (°C)	Freq. (Hz)	Avg. E* (MPa)	CV, E*	P-value (ANOVA)	95% C.I. for $\mu_{Control}$-μ_{BF} (MPa)
Control	4	10	21291	8.9%	0.0470	(48, 5165)
BF			18684	4.7%		
Control	21	1	8208	15.1%	0.0025	(1776, 5219)
BF			4710	14.1%		
Control	37	0.1	1753	9.1%	<0.0001	(1013, 1410)
BF			541	5.1%		

As shown in Table 11, the control mix exhibits statistically significantly greater stiffnesses at low temperature and high frequency, intermediate temperatures and frequency, and high temperature and low frequency. These results substantiate the findings of the master curves to be statistically significant at 95% confidence. Differences of means were evaluated using one-way analysis of variance (ANOVA) and includes coefficient of variations for tested means as a measure of data spread as well as 95% confidence intervals (C.I.) for the difference between mean dynamic modulus values of the control and BF mixes.

Master curves for both mixes compacted at 7% air voids and shifted to a standard reference temperature of 21°C are shown in Figure 8. These master curves reflect how the mixes are expected to perform in the early stages of the pavement's life as no long-term aging of the mix was done. Figure 8 also includes phase angle master curves of both mixes at 7% air void to assess the degree of viscous response under load through a range of reduced frequencies.

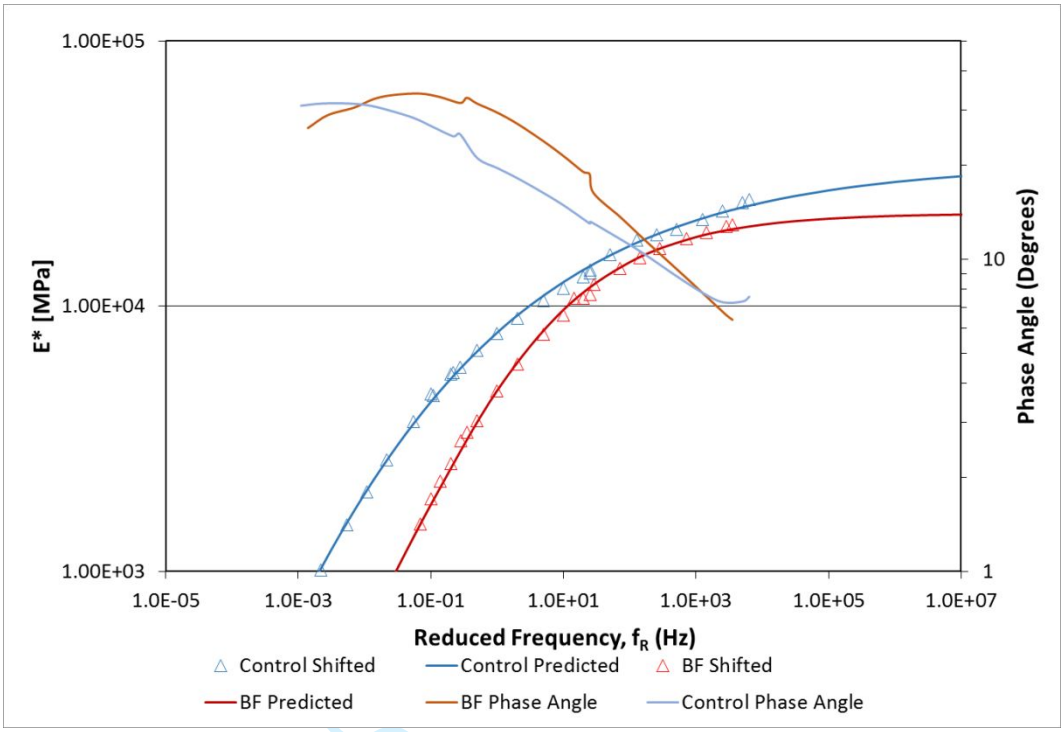

Figure 8: Mix Master Curves at 7% Air Voids

As seen in Figure 8, the control mix has greater estimated dynamic modulus values at frequencies of about 5E-05 and greater. At 7% air voids, the master curves show expectations of the control mix showing superior resistance to rutting at high temperatures (low frequencies). At low temperatures, the BF mix again graphically shows a greater resistance to brittle low temperature cracking (high frequencies). Table 12 shows statistical comparisons between mixes at critical temperature and frequency selections.

Table 12: Summary Statistics Between Binders at 7% Air Voids

Binder	Temp. (°C)	Freq. (Hz)	Avg. E* (MPa)	CV, E*	P-value (ANOVA)	95% C.I. for $\mu_{Control}$-μ_{BF} (MPa)
Control	4	10	22792	6.8%	0.0096	(1257, 6346)
BF			18991	8.9%		
Control	21	1	7910	4.7%	<0.0001	(2258, 3962)
BF			4799	14.6%		
Control	37	0.1	724	11.3%	<0.0001	(319, 544)
BF			292	17.8%		

As seen in Table 12, the control mix again portrays statistically significantly greater dynamic modulus values at all compared temperatures and frequencies. These results validate the trends shown in the master curves of Figure 8 as statistically significant differences among the binders at 7% air voids.

A comparison of mix stiffnesses within mixes at varying air void contents was also desired to assess if mixes undergo significant dynamic modulus variations during loading. These changes are not completely associated with changes over the life of the pavements as binder aging conditions were not varied with air void contents. Results of the within mix comparisons are summarized in Table 13.

Table 13: Statistical Summary Within Binders

Binder	AV, %	Temp. (°C)	Freq. (Hz)	Avg. E* (MPa)	CV, E*	P-value (ANOVA)	95% C.I. for $\mu_{4\%}$-$\mu_{7\%}$ (MPa)
Control	4%	4	10	21291	8.9%	0.2302	(-4203, 1201)
	7%			22792	6.8%		
	4%	21	1	8208	15.1%	0.6214	(-1066, 1662)
	7%			7910	4.7%		
	4%	37	0.1	1753	9.1%	<0.0001	(836, 1222)
	7%			724	11.3%		
BF	4%	4	10	18684	4.7%	0.7581	(-2631, 2017)
	7%			18991	8.9%		
	4%	21	1	4710	14.1%	0.8596	(-1268, 1090)
	7%			4799	14.6%		
	4%	37	0.1	541	5.1%	0.0002	(175, 323)
	7%			292	17.8%		

Table 13 shows that both mixes showed statistically significant increases in mean E* values at only high temperature (37°C) and low frequency (0.1 Hz) when the mix was compacted at 7% air voids and 4% air voids to understand the effect of post-construction consolidation. These results show that brittle cracking susceptibility should not vary significantly for either mix during densification; however, resistance to rutting increases during pavement densification as would be expected. The similarity in trends shows that the BF mix behaves similar to the control mix with regard to dynamic modulus changes due to the anticipated densification over the life of the pavement.

Because HMA mixes are composed of elastic and viscoelastic materials, it is important to also consider the mix phase angle in addition to the dynamic modulus. The phase angle (δ) varies from 0 to 90° and is a measure of the degree of elastic and viscous behavior within the mix under load. A lower phase angle indicates a greater degree of elastic behavior while a higher phase angle indicates more viscous behavior at the same complex modulus. The viscous component of the load response is attributable to energy loss through non-recoverable deformation while the elastic component of the load response is attributable to stored energy that is recoverable upon matrix relaxation (Huang, 2004). Figure 9 shows both mix's phase angle variations with dynamic moduli variations at 7% air voids. Phase angles at 4% air voids were not compared due to the inability to replicate the binder aging that will exist when the pavement is at 4% air voids and the great degree of impact binder aging has on the phase angle of the mix.

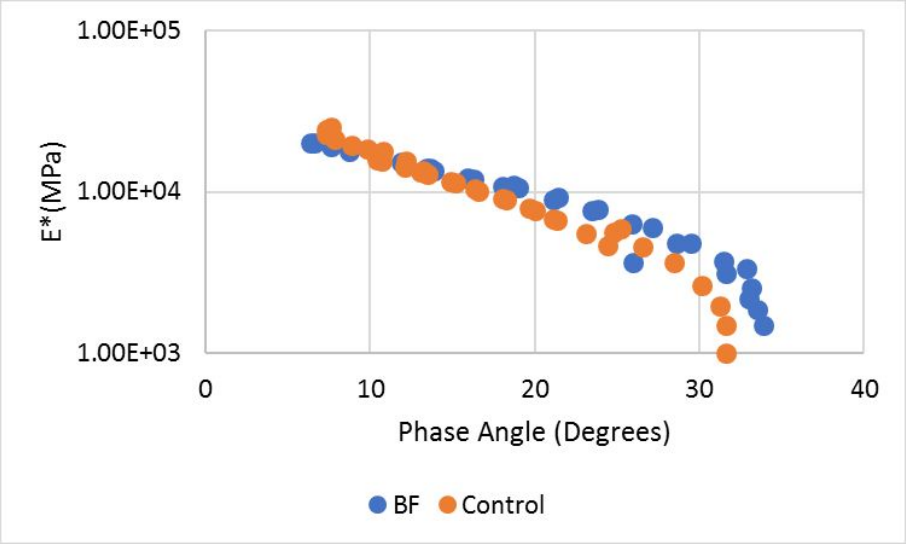

Figure 9: E* vs δ at 7% Air Voids

Figure 9 shows that the BF mix reaches a peak phase angle of 31° at a dynamic modulus of 1500 MPa while the control mix reaches a peak phase angle of 25° at a dynamic modulus of 1500 MPa. Both mixes trend the same with lower phase angles at the greatest moduli corresponding to low temperatures. As test temperatures increase and load frequencies decrease, the mix phase angles increase to a maximum and then began to decrease again at high temperatures and low frequencies. This decrease beyond maximum is likely attributable to an increased influence of aggregate interlock within the mixes as the binders began to display more viscous behavior beyond the linear viscoelastic region. A statistical analysis of phase angles at critical temperatures and frequencies is summarized in Table 14.

Table 14: Statistical Comparison Summary of δ at 7% Air Voids

Binder	Temp. (°C)	Freq. (Hz)	Avg. δ (°)	CV, δ	P-value (ANOVA)	95% C.I. for $\mu_{Control}$-μ_{BF} (°)
Control	4	10	7.3	1.0%	0.7068	(-2.4, 1.8)
BF			7.6	13.2%		
Control	21	1	19.6	0.5%	<0.0001	(-12.0, -7.7)
BF			29.5	4.8%		
Control	37	0.1	31.1	1.9%	0.1564	(-2.9, 12.5)
BF			26.3	18.1%		

Table 14 shows that the BF mix has a statistically significantly greater phase angle at intermediate temperatures and 1 Hz frequency. The mixes showed comparable phase angles at low temperature and high frequency. At high temperature and low frequency, the BF mix shows a slightly significantly lower phase angle. These analyses show that the BF mix exhibits a comparable ability to relax stress to the control mix at low temperatures, less ability to relax stress at intermediate temperatures, and potentially greater ability to relax stress at high temperatures. The more viscous response by the BF mix at intermediate temperatures (greater average phase angle) as compared to the control mix helps explain why

the BF mix exhibited a more rapid rate of damage accumulation in the beam fatigue testing presented earlier in this report.

B.5. Moisture Susceptibility

Compacted specimens for both mixes resulted in varying air void contents. In order to investigate and normalize TSR values, trends between air voids and measured peak strengths were determined for each specimen subset. These results and trends can be seen in Figure 10.

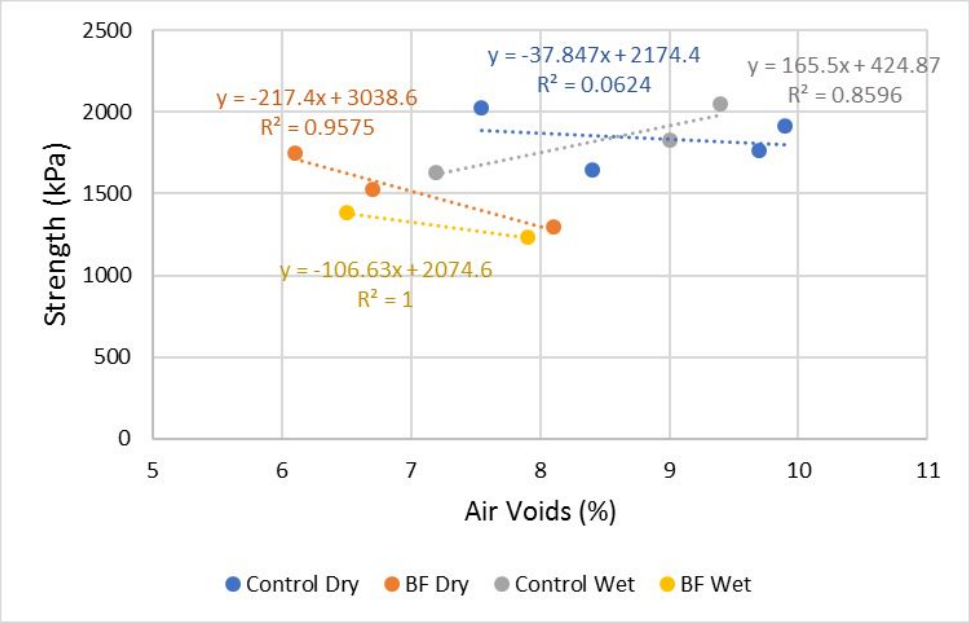

Figure 10: Air Voids vs. Peak Strength

Trends shown in Figure 10 were used to compare measured TSR values with TSR values calculated based on predicted peak strengths at the same air void content ($TSR_{adjusted}$). Because tensile strength is dependent on air void contents, wet and dry strengths at the same air void contents should be used to produce unbiased TSR ratios. Both TSR values are shown in Table 15 along with specimen pair average air void content and difference in respective air void contents between the wet and dry specimens. A TSR value of 1.0 indicates no moisture damage was incurred during one freeze-thaw cycle.

Table 15: TSR Value Comparison

Binder	Avg. AV (%)	ΔAV (%)	$TSR_{measured}$	$TSR_{adjusted}$
Control	7.4	0.4	0.80	0.87
Control	8.7	0.6	1.11	1.01
Control	9.6	0.7	1.16	1.11
BF	6.3	0.4	0.79	0.84
BF	6.6	0.2	0.90	0.85
BF	8.0	0.2	0.95	0.94

As shown in Table 15, both mixes show trends of increasing TSR with increasing air voids. To assess statistically significant trends, a one-way ANOVA and F-test modeling analysis was used. Results of the statistical testing show that a statistically significant difference occurs for air void content's role in TSR value (p=0.0414) and a non-statistically significant

difference occurs for binder's role in TSR value (p=0.5120). These findings suggest no significant difference in mix moisture susceptibility at the same relative air void content.

Both the peak strength trend equations shown in Figure 10 and strengths determined using linear regression modeling were used to interpolate TSR values for each mix at 7.0% air voids using the raw data at various air void contents summarized in Table 15. Equations shown in Figure 10 and linear regression predictions were performed on both wet and dry specimen strength data and respective strengths at 7.0% air voids were used to determine the TSR for each mix. For the control mix, the equations shown in Figure 10 estimate a TSR of 0.83 and the regression analysis estimates a TSR of 0.76 at 7.0% air voids. For the BF mix, the peak strength trends estimate a TSR of 0.87 and the regression analysis estimates a TSR of 0.88 at 7.0% air voids. These results imply that the BF mix provides a slightly greater resistance to moisture damage than the control mix. A standard recommended TSR value of 0.80 or greater is widely accepted as indication that a mix is sufficiently resistant to moisture damage (Asphalt Institute, 2014). By comparison, the control mix provides moderate-sufficient resistance to moisture damage while the BF mix provides sufficient resistance to moisture damage. Sufficient resistance to moisture damage may also be a good indicator of the degree of blending compatibility between the bio-derived binder and the RAP binder content as there was no significant strength loss through fracturing of binder to aggregate interfaces. Presence of black rock, or insufficient binder blending with the RAP binder content, often leads to increased stripping due to weak bond interfaces allowing for the easy diffusion of water (Zaumanis et al., 2014).

VI. SUMMARY AND CONCLUSIONS

A potential complete replacement of neat bitumen by a novel non-petroleum-based binder in use with 50% RAP by aggregate and bitumen weight was evaluated in this research. Mix evaluation focused on mixture performance with the independent variable being the binder. Low temperature DCT testing showed that both the control and BF mixes yield mean fracture energies greater than the recommended 400 J/m^2 at test temperatures 10°C above their respective low temperature binder grade. However, when tested at the same low temperature of -12°C, only the BF mix averaged fracture energies greater than 400 J/m^2. These findings show that the BF mix provides greater resistance to thermal cracking at lower temperature ranges due to the relative softness of the virgin bio-binder as compared to the control at low operative temperatures. Furthermore, the BF mix showed rather consistent mean fracture energies at both 4% and 7% air voids indicating that post-construction compaction alone will not increase thermal cracking potential for this mix.

Testing showed that at intermediate working temperatures, the BF mix performed similarly to the control mix with the BF mix showing only slight potential for higher rates of fatigue damage accumulation. These findings did not; however, imply that the BF mix will undergo greater percentages of fatigue cracking in the field than the control mix. The BF mix fatigue coefficients fall within industry-suggested bounds to prevent excessive fatigue cracking at working temperatures.

At high temperatures, flow number testing showed that while the BF mix portrayed statistically significantly lower mean FN values than the control mix, the BF mix still showed acceptable rutting resistance for 20-year design ESALs of greater than 10 million but less than 30 million. While the BF mix is of a softer grade than the control mix, the mix is still able to resist high temperature shear deformations.

During evaluation of mix moisture susceptibility, it was determined that the BF mix has statistically-similar resistance to moisture damage as the control mix at 7% air voids with a tensile strength ratio greater than 0.80. By direct comparison, the BF mix has a slightly greater predicted resistance to moisture damage than the control possibly due to the higher adhesion characteristics of the binder in a mix consisting of 50% RAP.

The overarching conclusion of this research is that engineering an asphalt mixture with a complete crude-derived binder replacement and incorporation of 50% RAP is possible. The novel pine-derived sustainable bio-binder passed industry standards for performance at a 20-year design ESAL level of greater than 10 million but less than 30 million at low, intermediate, and high temperature criterion. It is noteworthy to add that these performance tests and test criteria were developed for mixes using conventional petroleum-based bitumen. Therefore, the full advantages of this bio-binder may not be fully appreciated within the confines of these performance tests alone but rather the results prove that such mixes yield performance results sufficient to pass conventional specifications. Further work undertaken within the BioRePavation project has shown that when compared to traditional petroleum-based mixes for binder and surface courses such bio-asphalt mixes generally provides better environmental performance and exhibit promise for longer lifespans with less maintenance in a full-scale test scenario.

REFERENCES

1. FHWA, U.S. Department of Transportation Federal Highway Administration. “Reclaimed Asphalt Pavement in Asphalt Mixtures: State of the Practice.” *FHWA Publication No. FHWA-HRT-11-021*. April 2011.
2. National Center for Asphalt Technology (NCAT): *Hot Mix Asphalt Materials, Mixture Design and Construction, 3rd ed*., NCAT. 1991.
3. EAPA (European industry association), Asphalt in Figures, 2016. [www.eapa.org]
4. Ali, Hesham. “Long-Term Aging of Recycled Binders.” Florida International University: Civil and Environmental Engineering Department; submitted to the Florida Department of Transportation. July 2015.
5. Haghshenas et al. “Research on High-RAP Asphalt Mixtures with Rejuvenators and WMA Additives.” University of Nebraska-Lincoln: Nebraska Department of Roads Research Reports. September 2016.
6. Zaumanis et al. “Influence of Six Rejuvenators on the Performance Properties of Reclaimed Asphalt Pavement (RAP) Binder and 100% Recycled Asphalt Mixtures.” *Construction and Building Materials*. November 2014.

7. Kowalski et al. “Thermal and Fatigue Evaluation of Asphalt Mixtures Containing RAP Treated with a Bio-Agent.” *Applied Sciences, Vol. 7, Issue 3*. February 2017.
8. Jiménez del Barco Carrión, A., Pérez-Martínez, M., Themeli, A., Lo Presti, D., Marsac, P., Pouget, S., Chailleux, E., Airey, G. D. (2017). Evaluation of bio-materials’ rejuvenating effect on binders for high-reclaimed asphalt content mixtures. *Materiales de Construcción*, *67*(327), 1–11.
9. Jiménez del Barco Carrión, A., Lo Presti, D., Pouget, S., Airey, G., & Chailleux, E. (2017). Linear viscoelastic properties of high reclaimed asphalt content mixes with biobinders. *Road Materials and Pavement Design*, 1–11.
10. Biophalt patent US 8,652,246 B2
11. Pouget S. & Loup L. "Thermo-mechanical behaviour of mixtures containing bio-binders", Road Material and Pavement Design, vol.14, Special Issue EATA, pp. 212-226, 2013.
12. ASTM D2172. “Standard Test Methods for Quantitative Extraction of Asphalt Binder from Asphalt Mixes.” Standard Specifications for Transportation Materials and Methods of Sampling and Testing, Washington D.C., 2007.
13. ASTM D7906. “Standard Practice for Recovery of Asphalt from Solution Using Toluene and the Rotary Evaporator.” Standard Specifications for Transportation Materials and Methods of Sampling and Testing, Washington D.C., 2007.
14. Asphalt Institute. Asphalt Mix Design Methods, 7th Edition. MS-2. 2014.
15. AASHTO T 331-13. “Standard Method of Test for Bulk Specific Gravity (Gmb) and Density of Compacted Hot Mix Asphalt (HMA) Using Automatic Vacuum Sealing Method.” Standard Specifications for Transportation Materials and Methods of Sampling and Testing, Washington D.C., 2015.
16. AASHTO T 209. “Theoretical Maximum Specific Gravity and Density of Hot Mix Asphalt (HMA).” Standard Specifications for Transportation Materials and Methods of Sampling and Testing, Washington D.C., 2015.
17. Y.H. Huang. Pavement Analysis and Design. Second Edition, Prentice Hall, New Jersey, 2004.
18. ASTM D7313. “Standard Test Method for Determining Fracture Energy of Asphalt-Aggregate Mixtures Using the Disk-Shaped Compact Tension Geometry.” Standard Specifications for Transportation Materials and Methods of Sampling and Testing, Washington D.C., 2007.
19. AASHTO T 321. “Determining the Fatigue Life of Compacted Asphalt Mixtures Subjected to Repeated Flexural Bending.” Standard Specifications for Transportation Materials and Methods of Sampling and Testing, Washington D.C., 2017.
20. AASHTO T 378. “Determining the Dynamic Modulus and Flow Number for Asphalt Mixtures Using the Asphalt Mixture Performance Tester (AMPT).” Standard Specifications for Transportation Materials and Methods of Sampling and Testing, Washington D.C., 2017.
21. AASHTO TP 79-13. “Determining the Dynamic Modulus and Flow Number for Asphalt Mixtures Using the Asphalt Mixture Performance Tester (AMPT).” Standard Specifications for Transportation Materials and Methods of Sampling and Testing, Washington D.C., 2013.

22. AASHTO T 283-14. "Standard Method of Test for Resistance of Compacted Asphalt Mixtures to Moisture-Induced Damage." Standard Specifications for Transportation Materials and Methods of Sampling and Testing, Washington D.C., 2015.
23. W.G. Buttlar, S. Ahmed, E.V. Dave, and A.F. Braham. "Comprehensive Database of Asphalt Concrete Fracture Energy and Links to Field Performance." Paper presented at the 89th Annual Meeting of the Transportation Research Board, Washington, D.C., January 2010.
24. Cascione et al. "Laboratory Evaluation of Field Produced Hot Mix Asphalt Containing Post-Consumer Recycled Asphalt Shingles and Fractionated Recycled Asphalt Pavement." Asphalt Paving Technology 2011, Association of Asphalt Paving Technologies, Vol. 80.
25. S.H. Carpenter. "Fatigue Performance of IDOT Mixtures." Research Report FHWA-ICT-07-007, Illinois Center for Transportation, July 2006.
26. National Cooperative Highway Research Program. "NCHRP Report 673: A Manual for Design of Hot Mix Asphalt with Commentary." Transportation Research Board, Washington D.C., 2011.

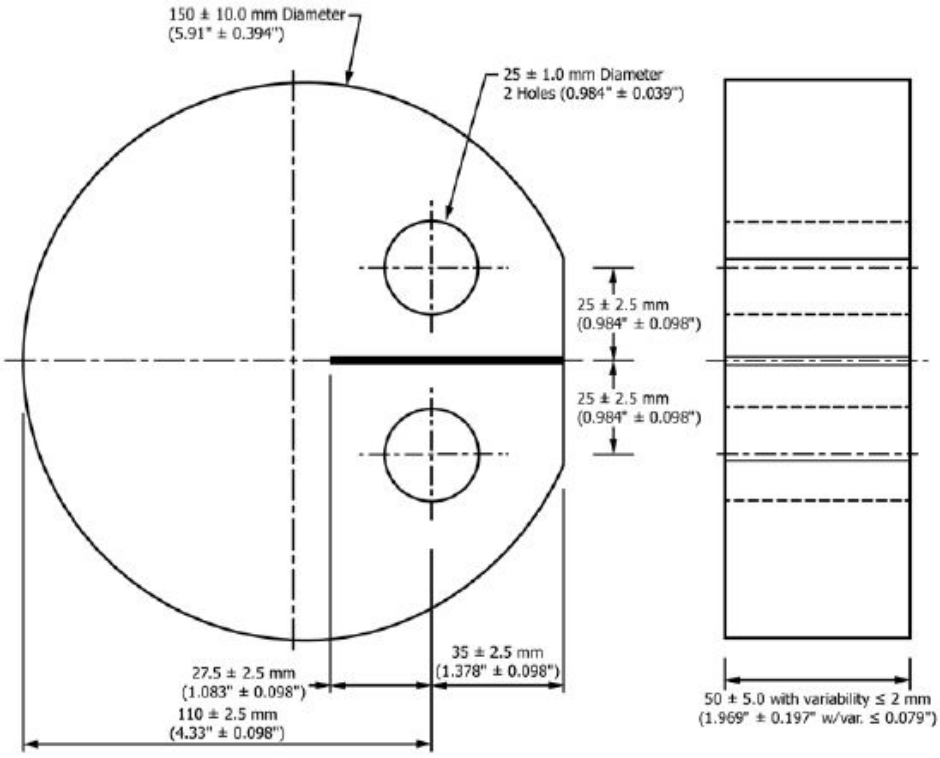

Figure 1: ASTM Standard DCT Specimen Dimensions (ASTM D 7313)

Figure 2: Beam Fatigue Testing Apparatus

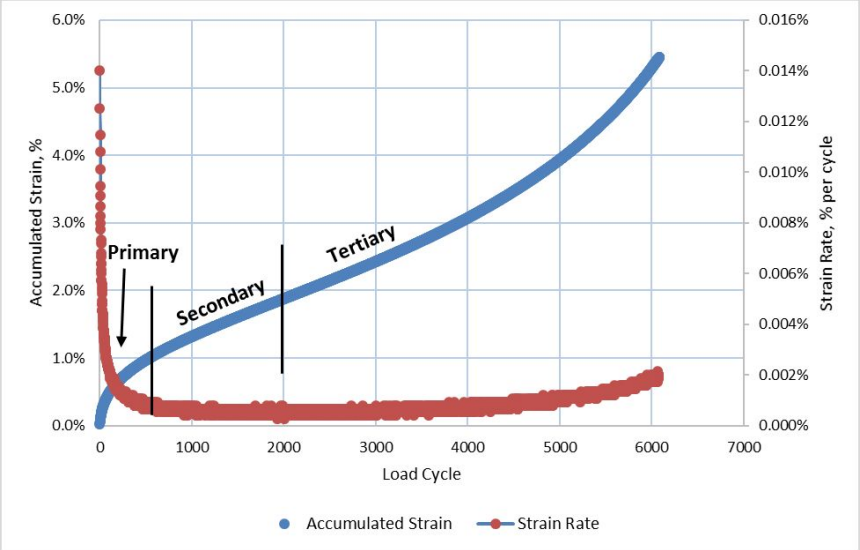

Figure 3: Example of Deformation Under Loading

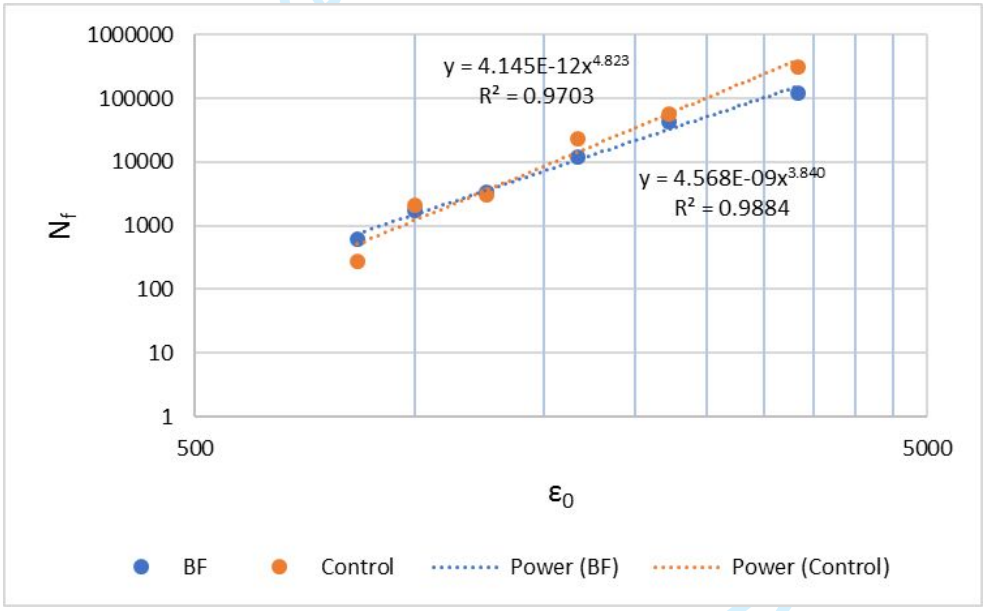

Figure 4. Fatigue Coefficient Determination

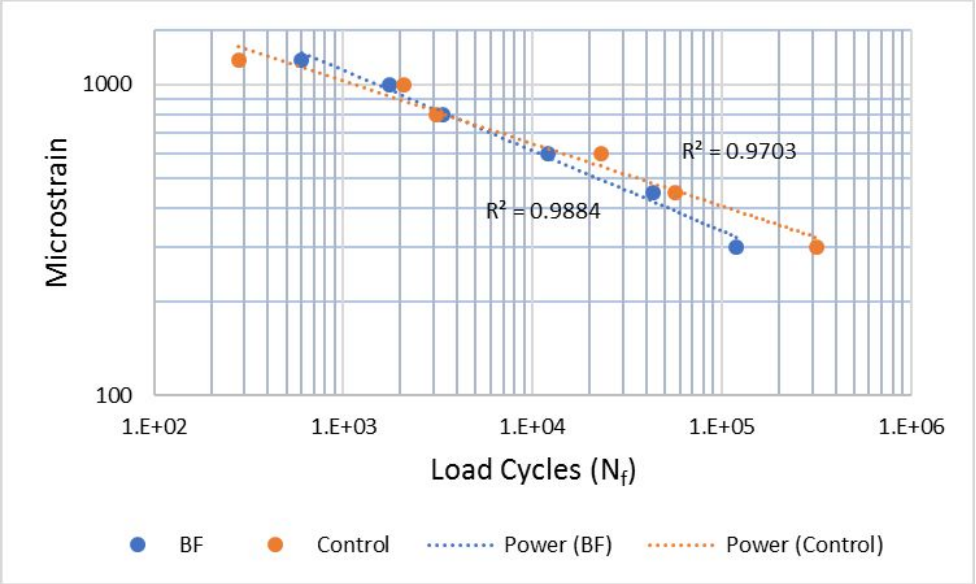

Figure 5. Fatigue Curves

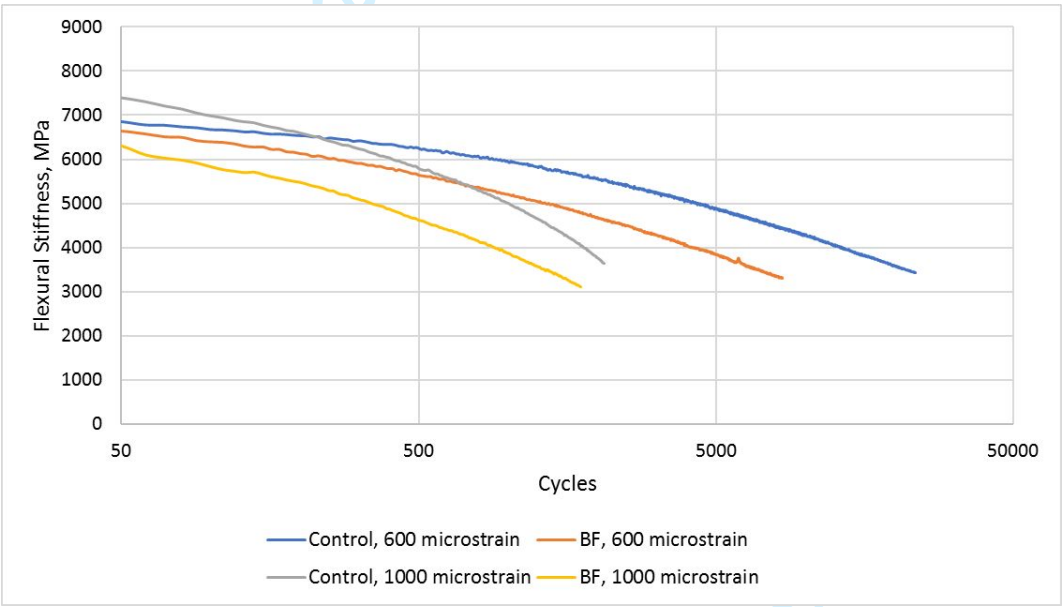

Figure 6: Flexural Stiffness Dissipation with Load Cycle Accumulation

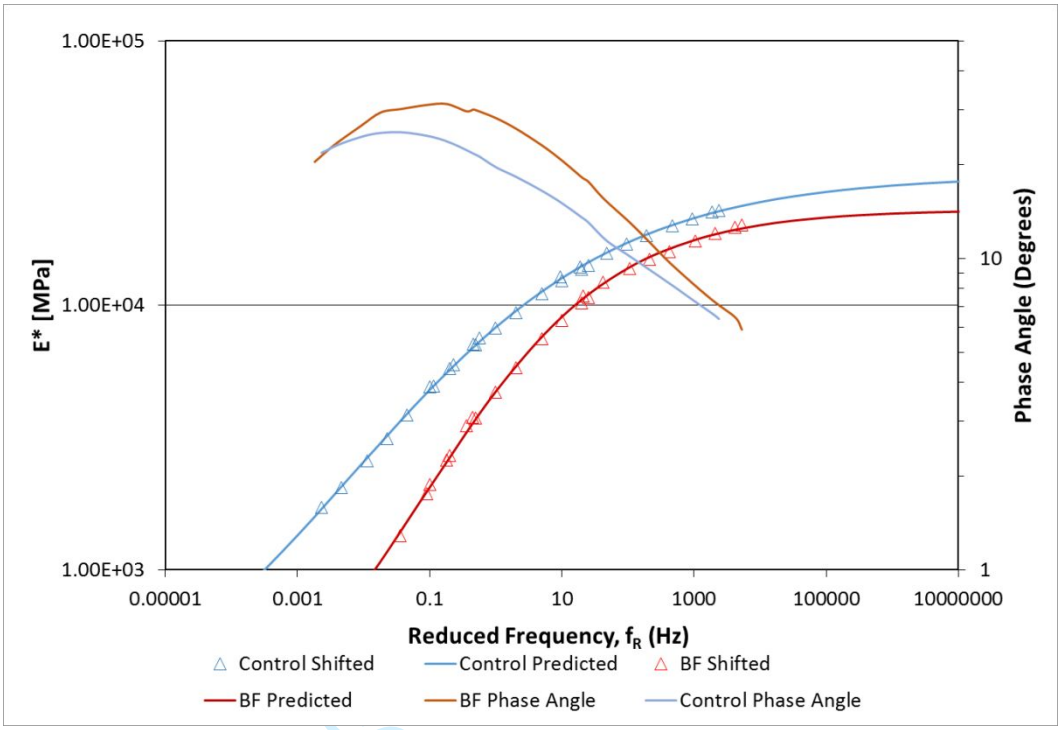

Figure 7: Mix Master Curves at 4% Air Voids

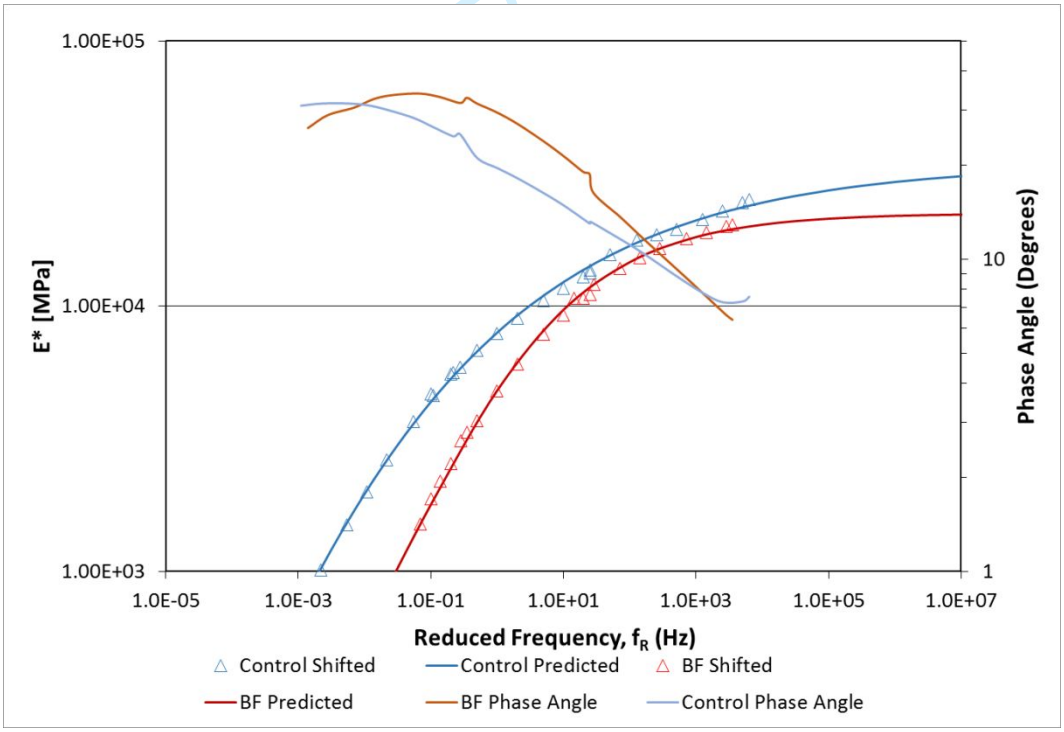

Figure 8: Mix Master Curves at 7% Air Voids

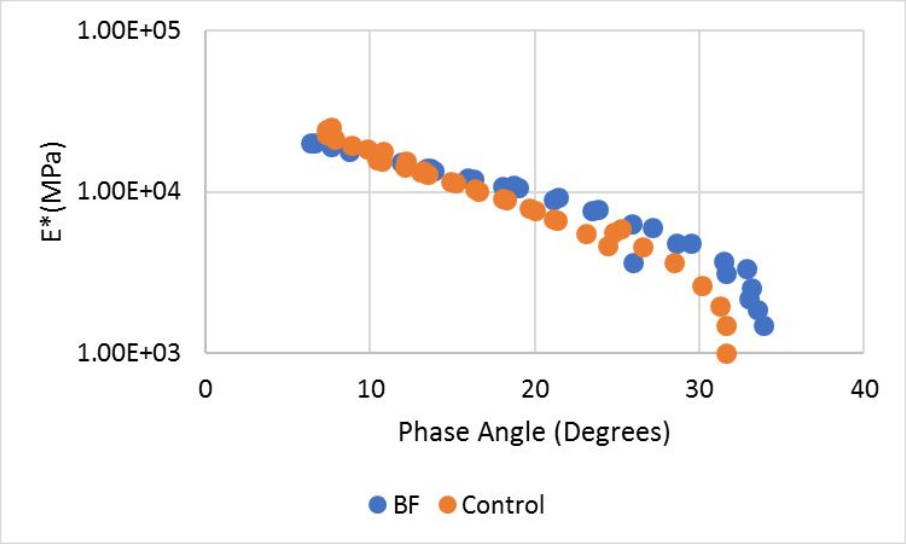

Figure 9: E* vs δ at 7% Air Voids

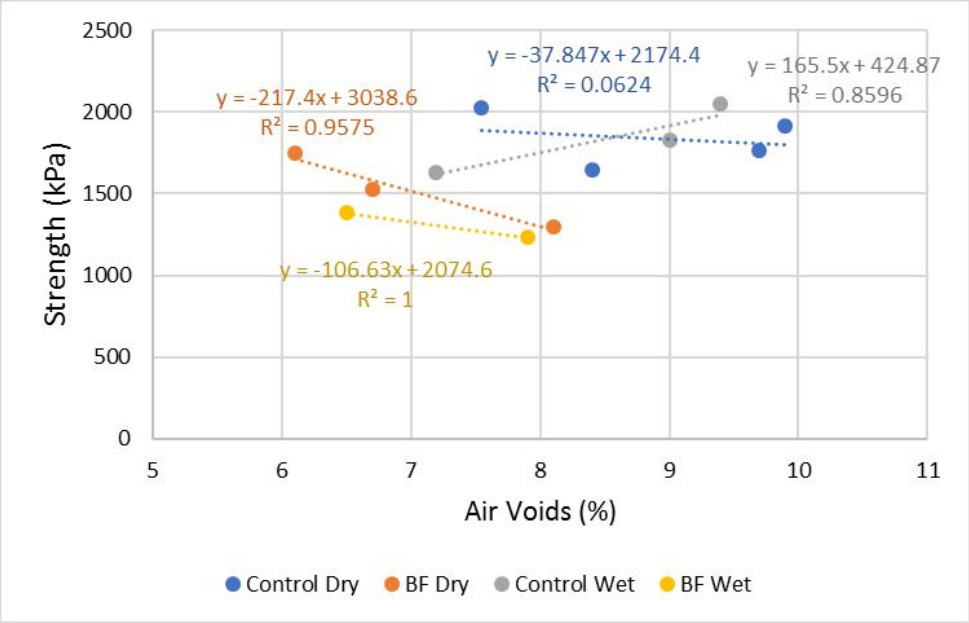

Figure 10: Air Voids vs. Peak Strength

Table 1: Binder PG Grade Summary

Binder	PG Grade	Penetration (x0.1mm)	Softening point (°C)	Fraass breaking point (°C)
Control	PG 64-22	55.0	49.0	-7
BF	N/A*	146.5	73.5	-15
RAP	PG 94-4	6.5	81.0	+14
Control + RAP	PG 76-16	25.0	61.8	+1
BF + RAP	PG 58-22	80.0	68.8	-7

Table 2: Aggregate Gradations

Sieve Size		Percent Passing			Requirements	
U.S. Customary	mm	Virgin	RAP	Blend	Min	Max
1”	25	100	100	100.0	100	
3/4”	19	98.9	99.9	99.4	90	100
1/2”	12.5	66.9	92.4	80.0		90
3/8”	9.5	29.6	60.6	45.5		
#4	4.75	23.5	29.9	26.8		
#8	2.36	22.6	24.7	23.7	23	49
#16	1.18	17.1	7.6	12.2		
#30	0.60	12.9	3.6	8.1		
#50	0.30	10.0	1.3	5.5		
#100	0.15	8.1	0.4	4.1		
#200	0.075	6.6	0.1	3.2	2	8

Table 3: Mixture Volumetrics

Property	Control	BF	Requirement
P_b	4.49	4.49	-
P_b (virgin)	2.8	2.8	-
P_b (RAP)	1.69	1.69	-
VMA	13.2	14.2	>13.0
VFA	69.5	71.6	65-78
DP	0.7	0.6	0.6-1.2

P_{ba}	0.8	0.4	-
P_{be}	3.7	4.1	-
G_{mm}	2.63	2.60	-
G_{mb}	2.52	2.50	-
$\%V_a$	4.0	4.0	4.0
G_b	1.047	1.035	-
G_{se}	2.831	2.799	-
G_{sb}	2.778	2.778	-

Table 4: DCT Testing Subset Parameters

Binder	% Air Voids	Test Temperature (°C)
Control	4	-6
	7	-6
	7	-12
BF	4	-12
	7	-12

Table 5: DCT Results Summary

Binder	Air Voids (%)	Test Temp. (°C)	Average G_f (J/m^2)	CV, G_f (%)	Average Peak Load (kN)
Control	4	-6	624	22.7%	3.77
BF	4	-12	599	23.6%	3.55
Control	7	-6	717	8.2%	3.73
Control	7	-12	383	9.8%	3.25
BF	7	-12	581	18.0%	4.11

Table 6: Statistical Comparison Summary Between Mixes

Binder	Air Voids (%)	Test Temp. (°C)	Average G_f (J/m^2)	P-value (ANOVA)	95% C.I. for $\mu_{Control}$-μ_{BF}
Control	4	-6	624	0.8349	(-295, 346)
BF	4	-12	599		
Control	7	-6	717	0.1192	(-55, 329)
BF	7	-12	581		
Control	7	-12	383	0.0365	(-376, -20)
BF	7	-12	581		

Table 7: Statistical Comparison Summary Within Mixes

Binder	Air Voids (%)	Test Temp. (°C)	Average G_f (J/m²)	P-value (ANOVA)	95% C.I.
Control	4	-6	624	0.3525	$\mu_{Cl4\%}-\mu_{Cl7\%}$ (-339, 153)
Control	7	-6	717		
Control	7	-6	717	0.0011	$\mu_{Cl-6}-\mu_{Cl-12}$ (223, 446)
Control	7	-12	383		
BF	4	-12	599	0.8676	$\mu_{BF4\%}-\mu_{BF7\%}$ (-263, 299)
BF	7	-12	581		

Table 8. Fatigue Coefficients

Binder	K1	K2	R^2
Control	4.145E-12	4.823	0.9703
BF	4.568E-09	3.840	0.9884

Table 9: Statistical Comparison Summary

Binder	Average FN	CV, FN (%)	P-value (ANOVA)	95% C.I. for $\mu_{Control}-\mu_{BF}$
Control	863	6.2%	0.0050	(123, 447)
BF	578	20.9%		

Table 10: NCHRP Recommended FN Values (NCHRP Report 673, Table 8-20)

ESALs (Millions)	Minimum FN	Control 95% C.I. μ_{FN}	BF 95% C.I. μ_{FN}
<3	-	(779, 948)	(386, 771)
3 to <10	53		
10 to <30	190		
≥30	740		

Table 11: Summary Statistics Between Binders at 4% Air Voids

Binder	Temp. (°C)	Freq. (Hz)	Avg. E* (MPa)	CV, E*	P-value (ANOVA)	95% C.I. for $\mu_{Control}-\mu_{BF}$ (MPa)
Control	4	10	21291	8.9%	0.0470	(48, 5165)
BF			18684	4.7%		
Control	21	1	8208	15.1%	0.0025	(1776, 5219)
BF			4710	14.1%		
Control	37	0.1	1753	9.1%	<0.0001	(1013, 1410)
BF			541	5.1%		

Table 12: Summary Statistics Between Binders at 7% Air Voids

Binder	Temp. (°C)	Freq. (Hz)	Avg. E* (MPa)	CV, E*	P-value (ANOVA)	95% C.I. for $\mu_{Control}$-μ_{BF} (MPa)
Control	4	10	22792	6.8%	0.0096	(1257, 6346)
BF			18991	8.9%		
Control	21	1	7910	4.7%	<0.0001	(2258, 3962)
BF			4799	14.6%		
Control	37	0.1	724	11.3%	<0.0001	(319, 544)
BF			292	17.8%		

Table 13: Statistical Summary Within Binders

Binder	AV, %	Temp. (°C)	Freq. (Hz)	Avg. E* (MPa)	CV, E*	P-value (ANOVA)	95% C.I. for $\mu_{4\%}$-$\mu_{7\%}$ (MPa)
Control	4%	4	10	21291	8.9%	0.2302	(-4203, 1201)
	7%			22792	6.8%		
	4%	21	1	8208	15.1%	0.6214	(-1066, 1662)
	7%			7910	4.7%		
	4%	37	0.1	1753	9.1%	<0.0001	(836, 1222)
	7%			724	11.3%		
BF	4%	4	10	18684	4.7%	0.7581	(-2631, 2017)
	7%			18991	8.9%		
	4%	21	1	4710	14.1%	0.8596	(-1268, 1090)
	7%			4799	14.6%		
	4%	37	0.1	541	5.1%	0.0002	(175, 323)
	7%			292	17.8%		

Table 14: Statistical Comparison Summary of δ at 7% Air Voids

Binder	Temp. (°C)	Freq. (Hz)	Avg. δ (°)	CV, δ	P-value (ANOVA)	95% C.I. for $\mu_{Control}$-μ_{BF} (°)
Control	4	10	7.3	1.0%	0.7068	(-2.4, 1.8)
BF			7.6	13.2%		
Control	21	1	19.6	0.5%	<0.0001	(-12.0, -7.7)
BF			29.5	4.8%		
Control	37	0.1	31.1	1.9%	0.1564	(-2.9, 12.5)
BF			26.3	18.1%		

Table 15: TSR Value Comparison

Binder	Avg. AV (%)	ΔAV (%)	$TSR_{measured}$	$TSR_{adjusted}$

Control	7.4	0.4	0.80	0.87
Control	8.7	0.6	1.11	1.01
Control	9.6	0.7	1.16	1.11
BF	6.3	0.4	0.79	0.84
BF	6.6	0.2	0.90	0.85
BF	8.0	0.2	0.95	0.94